International Journal of Natural-Applied Sciences and ENgineering
(IJNASEN)
Vol.3 No.1 (2025) pp. 113–119

Research Article

A FLUKA-Based Study on the Effect of Boron-Enhanced Concrete on Secondary Neutron Dose under Proton Beam Loss Scenarios

Demet Sarıyer*

Manisa Celal Bayar University, Turgutlu Vocational High School, Turgutlu, Manisa, Turkey
Corresponding Author Email: demet.sariyer@cbu.edu.tr **ORCID:** 0000-0002-7803-111X

Abstract: In proton accelerator facilities, interactions between high-energy protons and target materials lead to the production of secondary neutrons over a broad energy spectrum. These neutrons generate complex radiation fields within accelerator tunnels and surrounding structural components, resulting in significant dose contributions with direct implications for personnel and environmental safety. In this study, the effects of concrete enhanced with ferroboron and boron carbide (B_4C) additives at concentrations of 5%, 10%, and 15% on secondary neutron dose distributions were investigated using FLUKA Monte Carlo simulations. The simulations were performed under proton beam loss scenarios at an energy of approximately 1000 MeV, and the shielding performance of the materials was evaluated by calculating the ambient dose equivalent, H*(10). The results demonstrate that boron-enhanced concretes provide a substantial improvement in neutron attenuation compared with standard concrete, thereby contributing to the development of effective and optimized shielding designs for proton accelerator facilities. This study offers a valuable reference for radiation protection considerations in high-energy accelerator environments.

Keywords: Proton accelerator; Secondary neutrons; Boron-enhanced concrete; Neutron shielding; FLUKA simulation

Received: *10 September 2025* **|** ***Revised:*** *30 November 2025* **|** ***Accepted:*** *23 December 2025* **|** ***DOI:*** *10.22399/ijnasen.30*

1. Introduction

In proton accelerator facilities, the interaction of high-energy protons with target materials leads to the production of secondary neutrons spanning a wide energy spectrum. These neutrons generate complex radiation fields within accelerator tunnels and surrounding structural components, resulting in significant dose contributions that pose serious concerns for personnel safety and environmental protection [1-4]. In particular, secondary neutron fields produced under proton energies on the order of 1000 MeV and beam loss scenarios are of critical importance due to the high radiation levels involved and the stringent shielding requirements they impose. Consequently, accurate modeling and effective control of secondary neutrons are essential for both the design phase and the safe operation of proton accelerator facilities [5-7]. The dose distributions generated by secondary neutrons in accelerator environments must be carefully evaluated not only to ensure occupational safety but also to protect the surrounding environment and public health. For this reason, the development of effective shielding solutions to control and mitigate accelerator-induced radiation remains a key objective within the framework of international radiation protection standards and regulations. In shielding design, the neutron attenuation performance of materials is optimized in conjunction with economic and structural considerations to achieve cost-effective yet reliable radiation protection solutions [1, 6-10]. In the radiation shielding design of proton accelerator facilities, the neutron attenuation and dose reduction capabilities of various materials are taken into account. Standard concrete is one of the most widely used shielding materials due to its high mechanical strength, cost-effectiveness, and inherent neutron attenuation properties [8-14]. However, to further enhance the shielding performance of concrete against neutron and gamma radiation, different additives are incorporated into the concrete matrix at specific weight

fractions. In particular, additives such as iron, ferroboron (FeB), and boron carbide (B_4 C) have been shown to significantly improve neutron attenuation performance. Iron contributes to enhanced photon and particle attenuation owing to its high atomic number and density, while boron-containing compounds such as ferroboron and boron carbide exhibit high efficiency in capturing thermal and low-energy neutrons. As a result, the energy-dependent shielding performance of concrete-based materials can be optimized, enabling effective attenuation of neutrons over a broad energy range [1, 6, 8-15]. Experimental studies on radiation shielding design are often limited due to high costs and complex implementation conditions. Therefore, Monte Carlo–based particle transport simulations are widely employed in the design and optimization of shielding systems for proton accelerator facilities. The FLUKA Monte Carlo simulation code, which incorporates detailed physical models for high-energy hadronic interactions and offers advanced capabilities for complex geometry definitions, enables accurate modeling of secondary neutron production, transport, and interactions with matter. In particular, ambient dose equivalent values (H*(10)) calculated using the FLUKA USRBIN scoring module serve as a critical indicator for the development of shielding designs that comply with radiation protection standards in accelerator environments.[15-19]. In this study, the effects of concrete configurations doped with 5%, 10%, and 15% ferroboron and boron carbide on secondary neutron dose distributions are systematically investigated using FLUKA-based simulations. The results reveal the influence of different additive types and concentrations on shielding performance and provide valuable insights for the development of safe, efficient, and optimized shielding designs in proton accelerator facilities. Accordingly, this work aims to contribute to the existing literature while also serving as a relevant reference for radiation safety considerations in the design of future high-energy accelerator installations.

2. Materias and Methods

In this study, a tunnel-type shielding geometry was constructed to evaluate the dose distributions of secondary neutrons generated under abnormal operating conditions in proton accelerator facilities with a proton energy of 1000 MeV. The shielding configuration consisted of standard concrete and concrete doped with boron carbide (B_4 C) and ferroboron (FeB) at weight fractions of 5%, 10%, and 15%. All shielding calculations and dose evaluations were performed using the FLUKA Monte Carlo particle transport code, employing versions 2011.2b and 2011.2c. The simulation framework was designed to accurately model secondary neutron production, transport, and interactions within the tunnel environment and surrounding shielding materials.

2.1 FLUKA Monte Carlo Simulation Design and Data Generation

The tunnel model was developed to investigate neutrons generated by the interaction of protons with a copper target under abnormal operating conditions. The proton beam was treated as a point source, and the abnormal operating scenario was modeled as a point beam loss. The corresponding beam loss was set to 10 W, which is equivalent to 6.24×10^{13} protons per second [1, 3, 10]. The proton energies and beam loss parameters used for the calculation of dose equivalents under abnormal operating conditions are summarized in Table 1.

Table 1. *Beam energy and loss used in shielding design.*

Beam Energy (MeV)	**Beam Loss (p/s)**
1000	0.624×10^{11}

To ensure that the dose rate outside the tunnel shielding surrounding the copper target remains below the prescribed regulatory limits, the shielding thickness in the simulation geometry was deliberately selected to be sufficiently large. A spherical geometry with a radius of 25 m was defined to allow for comprehensive particle transport and interaction within the surrounding environment. To terminate particle tracking and prevent artificial backscattering, a 1 m thick black-body boundary was implemented at the outermost layer of the sphere.Standard concrete and concrete mixtures doped with B_4 C and FeB at weight fractions of 5%, 10%, and 15% were employed as shielding materials, while the total shielding thickness was fixed at 24 m. Within the spherical shielding volume,

an air-filled tunnel with dimensions of 5 m × 5 m × 10 m was explicitly modeled to represent the accelerator tunnel region. A simplified schematic of the shielding geometry adopted for the numerical simulations is presented in Figure 1.

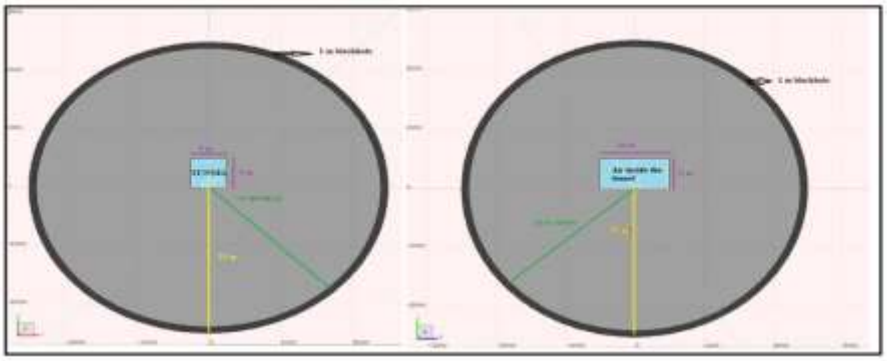

Figure 1. *Simplified geometry of the shielding configuration showing the cross-sectional view of the tunnel and surrounding shielding layers (left) and the longitudinal side view (right). The x-axis represents the horizontal direction, while the z-axis corresponds to the proton beam direction.*

During proton transport within the tunnel, copper was selected as the target material in regions where beam losses are expected to be concentrated, particularly on the inner surfaces of accelerator components. The target was modeled as a rectangular copper block with dimensions of 5 cm × 5 cm × 5 cm. In order to determine the maximum dose levels, a point source was positioned at the geometric center of the copper target. Furthermore, to prevent direct activation of the shielding material due to beam interaction, the beam axis was located at a distance of 2.5 m from the side walls and 4 m from the upper wall of the tunnel.Due to the statistical nature of Monte Carlo simulations, a large number of particle histories is required to achieve high accuracy. Therefore, to reduce statistical uncertainties, five independent simulation runs were performed using different random number sequences, each consisting of 6×10^8 primary particles. Owing to the large number of high-energy particles and the computational intensity of the simulations, all calculations were carried out using the TR-GRID national high-performance computing infrastructure.The simulation outputs were analyzed in detail using the FLUKA output files. The USRBIN scoring card was employed to evaluate dose values at various locations within the tunnel air and across different thicknesses of standard concrete as well as B_4 C- and FeB-doped concrete shielding materials. The detector dimensions were defined as 3400 cm, 3000 cm, and 1900 cm along the x-, y-, and z-axes, respectively, with corresponding numbers of bins set to 340, 300, and 190. This configuration resulted in detector voxel volumes of 10 × 10 × 10 cm^3.In the FLUKA simulations, particle fluences were converted into dose equivalents using FLUKA's built-in fluence-to-dose conversion coefficients through a convolution method applied within the USRBIN scoring framework. The proton energy was fixed at 1000 MeV, and the resulting dose distributions were visualized and analyzed using FLUKA's graphical user interface, FLAIR. Figures 2(a-b) present the dose distribution profiles of secondary neutrons generated by the interaction of 1000 MeV protons with the target material along the x-axis, both within the tunnel air environment and across the surrounding shielding, for different shielding materials. Specifically, Figure 2(a) illustrates the results for standard concrete and concrete doped with 5%, 10%, and 15% boron carbide (B_4 C), while Figure 2(b) corresponds to standard concrete and concrete doped with 5%, 10%, and 15% ferroboron (FeB). The dose rate (H) is expressed in micro sieverts per hour (μSv/h), and the radial distance (x) is given in centimeters (cm). Figure 4(a-d) illustrates the variation of the ambient dose equivalent rates of secondary neutrons produced by 1000 MeV proton–target interactions as a function of radial distance from the target center, evaluated both inside the tunnel air environment and within the surrounding shielding material. In all subfigures, a pronounced decrease in dose equivalent rates is observed with increasing radial distance. This general trend can be attributed to the combined effects of the geometric dispersion of the neutron flux and the multiple scattering, moderation, and absorption processes occurring within the shielding materials.

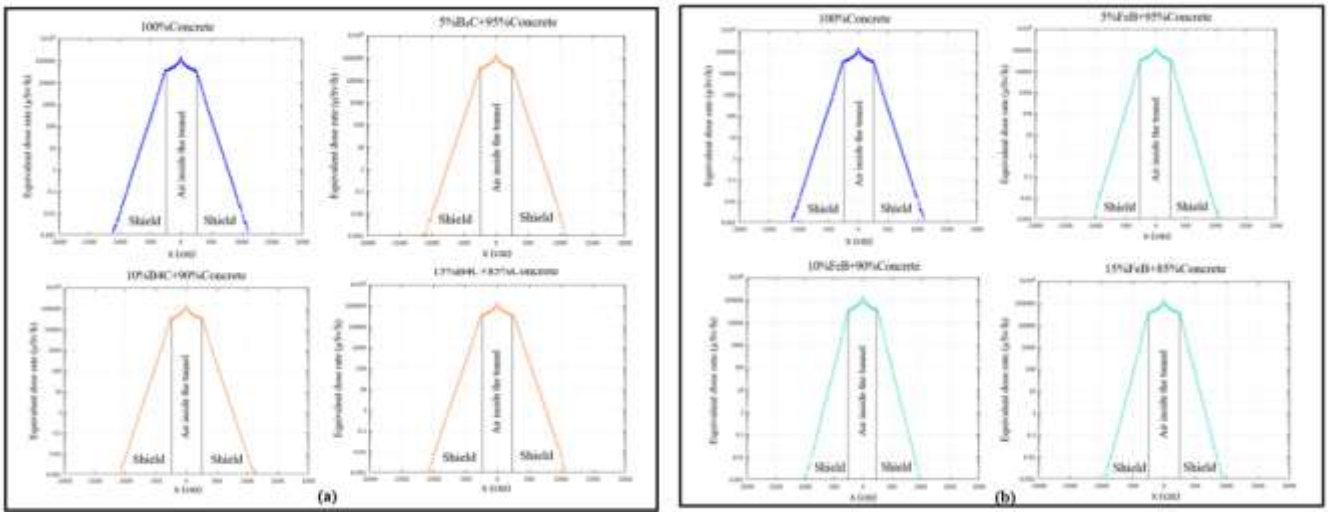

Figure 2(a-b). *Comparative representation of the radial distance–dependent ambient dose equivalent rates of secondary neutrons generated by the interaction of 1000 MeV protons with the target material: (a) standard concrete and concrete doped with 5%, 10%, and 15% boron carbide (B_4 C), and (b) standard concrete and concrete doped with 5%, 10%, and 15% ferroboron (FeB).*

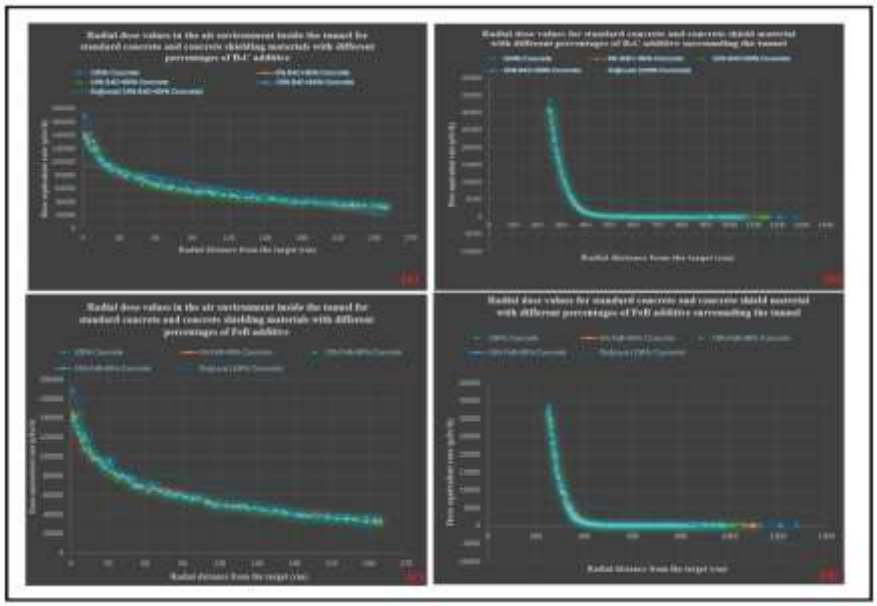

Figure 4. *Comparative presentation of the radial distance–dependent ambient dose equivalent rates of secondary neutrons generated by 1000 MeV proton–target interactions, evaluated within the tunnel air and the surrounding shielding:* ***(a)*** *air environment for B_4 C-doped concrete,* ***(b)*** *shielding environment for B_4 C-doped concrete,* ***(c)*** *air environment for FeB-doped concrete, and* ***(d)*** *shielding environment for FeB-doped concrete.*

For the tunnel air environment (Figs. 4a and 4c), the dose values are highest in regions close to the target and decrease progressively with radial distance for all shielding configurations. Standard concrete yields the highest dose levels, particularly near the target, whereas concretes doped with B_4 C and FeB exhibit a noticeable reduction in air-borne dose levels. Although the dose reduction achieved with a 5% additive content is relatively limited, it remains consistent compared to standard concrete. Increasing the additive ratio to 10% and 15% results in a more pronounced reduction in dose values, indicating enhanced neutron attenuation.The results obtained within the shielding material (Figs. 4b and 4d) more clearly demonstrate the effectiveness of the boron-based additives. While

standard concrete exhibits relatively high dose levels within the shielding, concretes containing B_4 C and FeB show a substantial decrease in dose equivalent rates across all radial distances. In particular, shielding configurations incorporating 15% B_4 C and FeB provide the lowest dose values throughout the shielding volume, indicating superior attenuation performance. The improved shielding efficiency of B_4 C-doped concrete can be attributed to the high thermal neutron capture cross section of boron, which is especially effective for absorbing low- and intermediate-energy neutrons. In contrast, FeB-doped concrete combines the neutron absorption capability of boron with the high density and scattering efficiency of iron, thereby contributing to the moderation of higher-energy neutrons. Overall, the results clearly demonstrate that increasing the boron-based additive content systematically enhances neutron shielding performance, leading to more effective radiation protection compared to standard concrete in both the tunnel air and shielding environments.

3. Results and Discussion

In this study, the ambient dose equivalent distributions generated by secondary neutrons produced through the interaction of 1000 MeV protons with a copper target were analyzed using FLUKA Monte Carlo simulations, both within the tunnel air environment and across the surrounding shielding materials. The shielding performances of standard concrete and concrete doped with different fractions of B_4 C and FeB were comparatively evaluated along both the linear direction (x-axis) and the radial distance from the target.Figures 2(a–b) present the dose distributions obtained along the x-axis within the tunnel air environment and inside the concrete shielding for a proton energy of 1000 MeV. For the standard concrete shielding configuration, relatively high dose levels are observed in regions close to the target, whereas a pronounced reduction in dose values is evident for concretes containing boron-based additives. In particular, increasing the additive content to 10% and 15% results in a much steeper decrease in dose levels compared to standard concrete. This behavior can be attributed to the high thermal neutron capture cross section of boron, which enables efficient absorption of secondary neutrons.Figures 4(a–d) illustrate the variation of radial ambient dose equivalent values of secondary neutrons as a function of the distance from the target center. In all subfigures, a monotonic decrease in dose equivalent values is observed with increasing radial distance for all shielding materials. This trend arises from the combined effects of the geometric dispersion of the neutron flux and the multiple scattering, moderation, and absorption processes occurring within the shielding materials.The radial dose profiles obtained for standard concrete exhibit higher dose levels, particularly in regions close to the target, whereas significantly lower dose values are achieved across all radial distances for B_4 C- and FeB-doped concretes. Although the dose reduction achieved at a 5% additive ratio is relatively limited, it provides a consistent improvement compared to standard concrete. As the additive content increases to 10% and 15%, the reduction in dose becomes substantially more pronounced. These results indicate that increasing the boron content strengthens the neutron absorption mechanism and significantly reduces the dose contribution from secondary neutrons.FeB-doped concretes demonstrate particularly notable performance in terms of moderating high-energy neutrons. The high density and scattering capability of iron contribute to the reduction of neutron energy, while the boron component within ferroboron efficiently captures the moderated neutrons. In contrast, B_4 C-doped concretes exhibit a more dominant effect in the absorption of low- and intermediate-energy neutrons. This distinction reveals that the two additives provide complementary shielding behavior across different neutron energy ranges.Overall, the concrete shielding configurations containing 15% B_4 C and FeB yield the lowest ambient dose equivalent values across all radial distances, both within the tunnel air environment and inside the shielding material. The results clearly demonstrate that increasing the fraction of boron-based additives systematically enhances neutron shielding performance and provides more effective radiation protection compared to standard concrete. These findings offer valuable guidance for the development of safe, efficient, and optimized shielding designs in high-energy proton accelerator facilities. Similar works reported in the literature [20-23].

4. Conclusion

In this study, the ambient dose equivalent distributions generated by secondary neutrons produced through the interaction of 1000 MeV proton beams with target materials were comprehensively evaluated using FLUKA Monte Carlo simulations for accelerator tunnels and the surrounding shielding structures. By comparatively

analyzing standard concrete and concrete shielding configurations doped with different fractions of B_4C and FeB, the effects of boron-based additives on neutron shielding performance were quantitatively assessed.The obtained results demonstrate that concretes enriched with boron-containing additives significantly reduce secondary neutron–induced dose levels compared to standard concrete. In particular, increasing the additive content leads to lower ambient dose equivalent values both within the tunnel air environment and inside the shielding material. This behavior indicates the presence of an effective attenuation mechanism arising from the combined action of boron's neutron capture capability and the interaction processes occurring within the concrete matrix.A comparative evaluation of B_4C- and FeB-doped concretes reveals that the two materials exhibit complementary shielding behavior across different neutron energy ranges. FeB-doped concretes provide an advantage in moderating high-energy neutrons, whereas B_4C-doped concretes are more effective in absorbing low-energy neutrons. These characteristics suggest that the use of boron-based additives at appropriate ratios enables the optimization of shielding designs according to specific radiation scenarios.In conclusion, this study demonstrates that boron-doped concretes represent a strong and effective alternative for controlling neutron-induced radiation under beam loss scenarios encountered in proton accelerator facilities. The presented findings contribute to the development of more efficient, reliable, and optimized shielding solutions from a radiation protection perspective and provide a solid foundation for future studies involving different proton energies, shielding thicknesses, and hybrid material configurations.

Author Statements:

- Ethical approval: The conducted research is not related to either human or animal use.
- Conflict of interest: The authors declare that they have no known competing financial interests or personal relationships that could have appeared to influence the work reported in this paper
- Acknowledgement: The numerical calculations reported in this paper were performed at TUBITAK ULAKBIM, High Performance and Grid Computing Center (TRUBA Resources).
- Author contributions: The authors declare that they have equal right on this paper.
- Funding information: The authors declare that there is no funding to be acknowledged.
- Data availability statement: The data that support the findings of this study are available on request from the corresponding author. The data are not publicly available due to privacy or ethical restrictions.

References

[1] Sariyer, D., & Küçer, R. (2020). Effect of different materials to concrete as neutron shielding application. *Acta Physica Polonica A, 137*(4, Special Issue: ICCESEN-2019), 477–480. https://doi.org/10.12693/APhysPolA.137.477

[2] Emikönel, S., & Akkurt, İ. (2025). Radiation shielding properties of B_2O_3 –Bi_2O_3 glass. *International Journal of Computational and Experimental Science and Engineering (IJCESEN), 11*(2). https://doi.org/10.22399/ijcesen.2157

[3] Soyal, H., & Sarıhan, M. (2025). Evaluation of radiation protection knowledge and attitudes of health services vocational school students participating in practice in radiated environments. *International Journal of Computational and Experimental Science and Engineering (IJCESEN), 11*(2). https://doi.org/10.22399/ijcesen.508

[4] Sağlam, F., & Çetin, B. (2025). Investigation of gamma shielding properties of some industrial materials. *International Journal of Computational and Experimental Science and Engineering (IJCESEN),* **11**(2). https://doi.org/10.22399/ijcesen.1357

[5] Liu, J. (2005). Nuclear reactions: Spallation physics and ADS target design. *Brazilian Journal of Physics, 35*(3B), 894–902. https://doi.org/10.1590/S0103-97332005000500048

[6] Sarıyer, D. (2017). *Proton hızlandırıcılarında tünel tasarımı için kullanılan farklı zırh maddelerinin doz dağılımlarına etkileri* (Doktora tezi). Manisa Celal Bayar Üniversitesi, Fen Bilimleri Enstitüsü, Manisa, Türkiye.

[7] Sarkar, P. K. (2010). Neutron dosimetry in the particle accelerator environment. *Radiation Measurements, 45*(10), 1476–1483. https://doi.org/10.1016/j.radmeas.2010.07.001

[8] Paul, M. B., Dutta Ankan, A., Deb, H., & Ahasan, M. M. (2023). A Monte Carlo simulation model to determine the effective concrete materials for fast neutron shielding. *Radiation Physics and Chemistry, 202*, 110476. https://doi.org/10.1016/j.radphyschem.2022.110476

[9] Waheed, F., Al-Sudani, M. A. M., & Akkurt, I. (2025). The experimental enhancing of the radiation shield properties of some produced compounds. *International Journal of Applied Sciences and Radiation Research (IJASRaR), 2*(1). https://doi.org/10.22399/ijasrar.1

[10] Sarıyer, D., Küçer, R., & Küçer, N. (2015). Neutron shielding properties of concrete and ferro-boron. *Acta Physica Polonica A, 128*(2-B), B-201. https://doi.org/10.12693/APhysPolA.128.B-201

[11] Sarıyer, D., Küçer, R., & Küçer, N. (2015). Neutron shielding properties of concretes containing boron carbide and ferro-boron. *Procedia – Social and Behavioral Sciences, 195*, 1752–1756. https://doi.org/10.1016/j.sbspro.2015.06.320

[12] Sariyer, D., & Küçer, R. (2018). Development of neutron shielding concrete containing iron content materials. *AIP Conference Proceedings, 1935*(1), 100003. https://doi.org/10.1063/1.5025991

[13] Barbhuiya, S., Das, B. B., Norman, P., & Qureshi, T. (2024). A comprehensive review of radiation shielding concrete: Properties, design, evaluation, and applications. *Structural Concrete*. https://doi.org/10.1002/suco.202400519

[14] Gharieb, M., Mosleh, Y. A., Alwetaishi, M., Hussein, E. E., & Sultan, M. E. (2021). Effect of using heavy aggregates on the high performance concrete used in nuclear facilities. *Construction and Building Materials, 310*, 125111. https://doi.org/10.1016/j.conbuildmat.2021.125111

[15] Rokni, S. H., Cossairt, J. D., & Liu, J. C. (2007). *Radiation shielding at high-energy electron and proton accelerators* (SLAC Report). Stanford Linear Accelerator Center.

[16] Hançerlioğulları, A. (2006). Monte Carlo simulation method and the MCNP code system. *Kastamonu Education Journal, 14*(2), 545–556.

[17] Ferrari, A., Sala, P. R., Fasso, A., & Ranft, J. (2005). *FLUKA: A multi-particle transport code*. CERN-2005-10, INFN/TC_05/11, SLAC-R-773. https://cds.cern.ch/record/898301

[18]Böhlen, T. T., Cerutti, F., Chin, M. P. W., et al. (2014). The FLUKA Code: Developments and challenges for high energy and medical applications. *Nuclear Data Sheets, 120*, 211–214. https://doi.org/10.1016/j.nds.2014.07.049

[19] IAEA. (2018). *Radiation protection and safety of radiation sources: International basic safety standards*. IAEA Safety Standards Series No. GSR Part 3.

[20]Günoğlu, K., & Akkurt, İskender. (2023). Gamma-ray attenuation properties carbide compounds (WC, Mo2C, TiC, SiC, B4C) using Phy-X/PSD software. *International Journal of Applied Sciences and Radiation Research* , *1*(1), 1–8. https://doi.org/10.22399/ijasrar.6

[21]Demet Sarıyer. (2025). FLUKA Monte Carlo Assessment of Fe_2B-Based Shielding Materials for Secondary Neutrons in a 1000 MeV Proton Accelerator. *International Journal of Computational and Experimental Science and Engineering*, *11*(4). https://doi.org/10.22399/ijcesen.4544

[22]Morad Kh. Hamad. (2025). Synergistic Evaluation of Ionizing Radiation Shielding in Novel Lead-Free Alloys Using Geant4 MC toolkit. *International Journal of Applied Sciences and Radiation Research* , *2*(1). https://doi.org/10.22399/ijasrar.47

[23]AYDIN, H., SÜSOY DOĞAN, G., TEKİN, H. O., ŞEN BAYKAL, D., & İLTUŞ, Y. C. (2025). Examining the Neutron and Gamma Attenuation Characteristics of Various Amorphous Structures with Bioactive Properties. *International Journal of Computational and Experimental Science and Engineering*, *11*(3). https://doi.org/10.22399/ijcesen.2176